r

XMM Optical Monitor

MULLARD SPACE SCIENCE LABORATORY
UNIVERSITY COLLEGE LONDON

Author: Hajime Kawakami

Blue Detector Calibration Plan

DOCUMENT: XMM-OM/MSSL/SP/~~00 ??~~ 0067 20-Mar-95

20 March 1995

Blue detector calibration plan [Qualification Phase]
XMM-OM/MSSL/SP/00??

I. Optical Test Equipment

The blue detector, photon counting imaging detector, consists of two components, namely an image intensifier and a CCD. Most of the performances are dictated by the image intensifier. Test items associated with the image intensifier are described in section II. Non-negligible effects, however, will appear if the CCD has imperfections ("XMM-OM/MSSL/TC/ 0031.01", Oct.'94). Test items associated with CCD are described in section III. Overall performances, mainly affect of overlapping events, are in section IV. As all of the tests will be performed using a non-vacuum OGSE and a vacuum monochrometer, both testers are described first in this section.

<< non-vacuum OGSE >>
has been established for the blue detector. Items in the wavelength range of 250-550nm will be tested by this equipment. It consists of a large light tight box, 3 colour light source in a compact box, mask patterns, a high precision x-y table, 3 lenses and 3 appropriate attachments. The optical tester is vertically aligned for the mechanical stability of the detector and larger travel length of the x-y table.

Blue(460nm) and red(630nm) light is emitted by LEDs and green(530nm) by a fluorescence panel. The brightness in all colours is tuneable from zero to a high level by changing the voltage. The light level should be monitored for an accurate measurement, as the stability and the repeatability are 8% in the worst case.

A mask pattern is fitted on the compact box and projected onto the detector. The size of the masks is 40x40mm. There are 3 mask patterns; two 11x11 pinhole arrays with the diameters of 27um and 125um, and a photgraphic plate of a sky image. One of the mask patterns is selected depending on which experiment, and occasionally ND filters are used.

The x-y table is controlled by a UNIDEX-12 interface, which is accessed manually or from a computer through RS-232. The travel length is 150mm and the sensitivity is 0.2um/digit. The backlash of the x-y table was measured with CCD camera fed to a microscope, and was found to be 0.8um. The long range linearity accuracy is difficult to measure. The data sheet specifies 1um error over 25mm travel.

There are 3 lenses, a Relay lens x0.586 F/2 borrowed from La Palma Observatory, a Nikon EL 50mm F/2.8 lens and a Tominon 35mm F/4.5. The relay lens is used as a standard configuration, as it allows good resolution over the full detector area. As the magnification is about half and the lens is fixed to the detector, the mask image on the detector can be positioned with an accuracy of 0.4um. The spot size 27um is reduced to 13.5um on the detector. The size of the mask pattern, 40mmx40mm, is large enough to cover the full detector image area 18mmx18mm. The Nikon lens is used for resolution test, as it allows good resolution over an optical wavelength range 400-660nm and larger minification 1/5 (figure 1). The resolution measured by a microscope was 3um in orange light and 2.5um in green. The pinhole size of 27um is reduced to 5.4um on the detector. It also delivers the spot image on the detector with the position accuracy of 0.16um, as the lens is fixed to the detector rigidly. The mask pattern covers only 8mmx8mm on the detector at a time because of the strong reduction. But, the image can be delivered to the edge of detector except the 4 corners by the x-y table. The compact Tominon lens is used for the global distortion test, as it can be fed to the x-y table and be moved with the light source (Figure 2). The position accuracy of the image on the detector is completely dependent on the x-y table, namely 1um over 25mm travel. The resolution of the lens measured by the microscope is 10um. The reduction of the image is 2.

<< vacuum Monochrometer >>
also have been established for the measurement of R.Q.E. A Seya-Namioka type mounting is employed with a radius of curvature 300mm and F/5.6. There are 2 gratings; 1200 and 600 grooves/mm. The grating of 1200 grooves/mm covers wavelength from 0 to 500nm with dispersion of 2.5-2.7nm/mm. The grating of 600 grooves/mm is used only for the measurement in NIR region up to 1um. As slit width is opened no more than 50um, the wavelength resolution is about 0.1nm without optical aberration. The resolution is actually dictated by the shift of focal position, particularly in the longer wavelength ~500nm, which causes 0.5nm wavelength blurring. Even with the other optical aberration, wavelength resolution of 1nm is easily achieved. There are 2 light sources, a halogen lamp and a deuterium lamp. The halogen lamp offers stable and flat spectrum at >400nm, while the deuterium lamp offers high intensity in the UV region. Several order sort filters and attenuaters are implemented in the 3 filter wheels of the monochrometer. The rotations of the grating, hence wavelength, and the filter wheels are controlled by a computer. The light beam emitted from the monochrometer is redirected toward a photomultiplier or toward the blue detector by a chopping mirror. The light intensity is measured by the photomultiplier and the blue detector in turn for the Q.E. measurement. The Q.E. of the photomultiplier was calibrated by Thron EMI in September 1992. Diaphragms with the diameter of 10mm are inserted in front of both detectors at the exact distance from the exit slit. Both detector are operated in photon counting mode.

II. Image Intensifier

The blue detector employs a centroiding technique to achieve both of large pixel format and high time resolution. The typical extent of photo event is 3 CCD pixels. The center of gravity of an individual event is calculated accurately and quickly by a hardware, and the position is re-mapped to a subpixel whose size is 1/8 of CCD pixel. This technique enables high spatial resolution (<20 um) independent of the event size on the phosphor screen. Since CCD pixel format 256x256 is enough to create 2048x2048 sub-pixel, fast frame rate is also realized (Fordham et.al. 1992 ESA SP-356). But, sharp, stable and uniform event shape as well as narrow pulse height distribution are required for accurate centroiding, in other word the highest quality image tube is needed. Otherwise, image blurring and systematic modulation pattern appear (Kawakami et.al. 1994 NIM-A).

[1] P.H.D.

The detector is illuminated by a flat field, and an individual event in a CCD snap frame is analysed to get pulse height. The configuration shown in figure 2 but without the Tominon lens is suitable for this test. The light source is turned down to reasonable intensity. Optimum HV setting is determined so as to get sharp valley and peak (Figure 3), and also peak position ~80ADC, valley position ~30ADC.

As the flight model HV may have non-negligible ripple, the pulse height distribution is investigated by changing the HV to the 2nd/3rd MCP by +/-10V .

XMM-OM has 2 modes, imaging mode and fast mode. The latter employs the smaller window format for the faster frame rate. An event may lose energy in the fast mode due to the very short exposure time of a CCD frame and the fairly long decay time of the P-20 phosphor. The peak position of the pulse height distribution may move toward the lower energy and the valley may disappear. The pulse height distribution is measured in the fast mode to find the usable shortest frame rate.

The pulse height distribution is different for a diffuse light source and a point light source in a high count rate (pore paralysis). The 27um pinhole array is projected on the detector with the configuration shown in figure 1. A pulse height distribution is made from photo-events on pinholes changing the count rate. This measurement gives the observable brightest star.

[2] Dark Current

The detector input window is covered with a blackout material and the light source and the room lamp are turned off. Then, 24 hours integration is undertaken in 2048x2048 pixel format keeping the room temperature 28 degree Celsius. The temperature of the detector window is monitored by a stick-on thermocouple (e.g.PR6462B/00) during the exposure. Average dark current, global uniformity and hot points are quantified. The dark frames are measured 3 times with an interval of 1 week, as the dark current reduces gradually. The dark current is sometimes caused by optical feed back from the fluorescence in the MCP (figure 4). In such a case, short time decay of dark current is not expected. The dark image also give the information on dead pores (figure 5). As the detector is not illuminated, the dark spots cannot be due to dust nor contamination on the input window.

[3] Turn-on Channel

Another 24 hours integration is undertaken with the same setting as the dark current, but with the photo-cathode voltage off. There are scattered events over the full imaging area, as MCP pores respond to cosmic rays, but pixels with more than 100 events are associated with turn-on channel of MCP (figure 6). The number of turn-on channel indicates the life time of the tube and quality control of the manufacturing.

[4] Sensitivity uniformity <photon counting mode>

A flat field image is acquired in central 18mmx18mm for 24 hours with the pixel format 2048x2048 in the photon counting mode. The optical setting is shown in figure 2 but without the Tominon lens. Blue and red LEDs and green fluorescence panel are used as wide band light sources. Monochromatic light with the band width of 1nm is delivered from the vacuum monochrometer through an UV optical fiber. The wavelength range is 250-550nm. The light level is turned down to 5000 events/sec over full detector area to avoid event overlapping. Global non-uniformity (figure 7), local dead/bright points and optical interference pattern are investigated. A new attachment to the monochrometer and the OGSE are necessary for the UV fiber.

[5] Sensitivity uniformity <analog mode>

The uniformity of the photocathode is shown well by the flat field image in the photon counting mode. But, overall gain including photocathode sensitivity, MCP gain, uniformity of phosphor, transparency of the tapered fiber block and sensitivity of CCD are shown by a simple analog image accumulated in the CCD (figure 8). Since the photon count rate must be low to avoid MCP pore paralysis, 100 000 CCD snap frames are summed inside a computer to get adequate S/N. The green fluorescence panel is used for the light source. Global uniformity, bright pores, dark pores, granulation of phosphor and the effect of fiber bundles are investigated.

[6] Resolution

The 11x11 pinhole array with 27um diameter is projected on the detector with the magnification of x1/5 as shown in figure 1. The pinhole size is expected to be 5.5um on the detector. The central 5x5 pinholes are used for determination of resolution to minimize the effect of the curved window of the detector (figure 9). The poor spatial sampling by the MCP pore might give different resolution place by place. Averaging 25 spots may level off the effect and also gives better S/N. As the resolution is mainly dictated by the proximity gap of the photocathode, the better resolution is expected for the longer wavelength light and for the higher photocathode voltage (figure 10). Resolutions for the different colour (250-550nm) and different voltage (50-300V) are measured in the OGSE.

The wavelength range of XMM-OM specification is down to 170nm, which is vacuum UV region. The resolution in the wavelength shorter than 250nm is measured inside the vacuum monochrometer.

The up grading of the OGSE is necessary to deliver UV light as stated in [4]. Two new lenses, one for the NUV in the OGSE and the other for

VUV in the monochrometer, are under design by RH. As the lens for VUV has colour aberration, the position of the mask pattern must be moved in the monochrometer.

other factor limiting the resolution is the shape of individual events. If the shape changes event by event, for instance satellite events around the main event (see [10]), the centroiding accuracy is degraded crucially. This caused 70um image blurring in some dirty image intensifiers. If subpixel size is taken to be 1um for instance instead of 9um of the current MIC system, the pore structure of the 1st MCP is clearly resolved (figure 11) by a quality image intensifier. As the super fine subpixel format is not available in hardware, 1 million CCD snap frames are analysed by the computer and are mapped into subpixel space. This experiment can certify that the proximity gap of the photocathode dominates for the resolution.

[7] Position accuracy

The global distortion of the detector is measured in the configuration shown in figure 2. As the compact lens moves with the x-y table, position accuracy is completely dependent on the x-y table's accuracy, which is 1um over 25mm travel. The 11x11 pinhole array with 125um diameters is used for the proper spot size on the detector to determine the position accurately. The x-y table is travelled step by step and cover the full 18mmx18mm area . The effect of the curved window is co. ected by calculation. The smallest iris of the lens, F/16, is used for minimizing image blurring due to the shift of the focus at the edge of the curved window.

The local but very fine position sensitivity is measured in the configuration shown in figure 1. The 11x11 pinhole array with 27um diameters is used to give very small spot image on the detector and is moved over 3 CCD pixels with a step of 0.5um on the detector. As the minification is 5 and the backlash of the x-y table is 0.8um, a pinhole position on the detector can be controlled with an accuracy of 0.16um. Position sensitivity in the sub-micron level with 100 micron dynamic range is determined. The effect of MCP pores may also be found. An example of this kind test is shown in figure 12.

[8] Detectable Quantum Efficiency

The detector is attached to the vacuum monochrometer and illuminated by monochromatic light ranging from 150-550nm with a step of 10nm. The total count is compared with the calibrated photomultiplier. The light beam is switched to one of the detectors by a chopping mirror. Di. hragms with a diameter of 10mm are located in front of the both detectors at exactly same distances from the exit slit. The light level is tuned no more than 30 000 count/s in the blue detector. The attenuation of light, order sort filter and wavelength are controlled by an IBM-PC. The outputs of the both detectors are also acquired by the IBM-PC. The chopping mirror is, however, rotated manually. The deuterium lamp and the grating with 1200 grooves/mm are used over the full wavelength range. The width of entrance slit is narrower than 20um and the exit slit than 50um. The wavelength resolution is better than 1nm. The observation sequence at one wavelength consists of (1) 3x10sec exposures by MIC, (2) 10sec dark current by MIC, (3) 3x10sec exposures by PM, (4) 10sec dark current by PM, (5) 3x10sec exposures by MIC, (6) 10sec dark current by MIC, (6) 3x10sec exposures by PM, (8) 10sec dark current by PM. The chopping mirror is rotated during the dark current measurements. The 6 redundant measurements give the information on accuracy. The internal error is expected to be smaller than 0.3% in units of Q.E. over the wavelength range (figure 13). The absolute quantum efficiency is completely dependent on the calibration of the photomultiplier. As the last calibration was done in 1992, re-calibration may be necessary because of the aging effect and also heavy duty usage.

[9] Event Shape

As the expected event size corresponds to 1.0 CCD pixel, the event profile is not resolved in a snap frame of the normal configuration. A tapered fiber block is inserted between the CCD and the output of the image intensifier to magnify the image by x3. Then, snap frames are captured by the CCD and analyzed to measure the event width and el psity. As the higher energy event has the larger size, events are classified into 10 groups according to their energy and added together. 100 events are enough to make high S/N standard profile for each energy group (figure 14). Event size must be less than 70um, as the large event size causes the larger probability of overlapping. The event shape must be round, as an elliptic event shape causes systematic error in centroiding.

[10] Satellite Events

Tiny but non-negligibly bright spots appear around the main event in some image tubes (figure 15). These cause the inaccuracy of centroiding and also increase the probability of overlapping. The satellite events often appear at the boundary of the main event. An event is subtracted by the standard profile of the corresponding energy group, and the deviation is derived. The deviation is mainly due to the satellite events, but may be due to an amoeba-shaped extended halo. Any deviation is characterized statistically (e.g. energy/event, distance from the main event). The level of the deviation should be confirmed to be negligible.

[11] Moire Fringing

is obvious from figure 11 that the poor spatial sampling of the MCP pore limits the quality of the image. Moire fringing pattern sometimes appears in high S/N flat field beating with subpixel spacing (figure 16). If the pattern appears, another flat field image is observed with rotating CCD to make sure whether the pattern is simply due to photocathode sensitivity distribution or due to the beat between hexagonal pattern of MCP pores and subpixels. The relation of S/N to the number of photon is investigated using local 128x128 pixels, as the S/N is not always equal to the square root of photon number if poor spatial sampling is dominant.

[12] Non-Uniformity of Pulse Height Distribution

The brightness of a flat field is lower at the edge of the detector in analog mode in some intensifiers. Image area is divided into 8x8 sectors and pulse height distributions are derived separately for different sectors. The peak position at the boundary sector is less than half of the central sector and the valley disappears in one intensifier, while the distribution is very uniform in other intensifier (figure 17). As the bad pulse height distribution causes photometric inaccuracy, the un ormity must be confirmed.

[13] Non-uniformity of CCD pixel based modulation

Not only the pulse height distribution but also event shape changes place by place in some intensifiers. As the centroiding requires precise stability of event shape, the variation of the event shape causes grid pattern corresponding to the CCD pixel. Figure 18 shows the flat field image at the edge of the tube, when the centroiding LUT is tuned at central area. This degraded image often causes the DPU to fail to correctly identify guiding stars.

The event width distributions are derived separately for different sectors and the uniformity is checked. Also, it should be confirmed the modulation pattern does not appear in neither the image center nor boundary.

[14] Currents

consumed by photocathode, 1st MCP, 2nd/3rd MCPs and anode are measured and to be confirmed that all are less than 15uA.

[15] Stability

Pulse height distribution is monitored every 1 hour over 24 hours after 24 hours warming up. The CCD base modulation pattern is also monitored every 1 hour by observing a flat field.

[16] Life time test
The image intensifier is illuminated by a flat field with the count rate of 1 million count/s over the full area for 1 week. And measure (1) Q.E. (2) pulse height distribution (3) currents and (4) satellite ev ts.

III. CCD

[17] Sensitivity uniformity
The CCD camera is attached to the OGSE in the configuration shown in figure 2 but without the Tominon lens, which creates a flat field image on the CCD. The green fluorescence panel is used as a simulated light of P-20 phosphor. The light level is turned up until the CCD out shows the half of full scale of the ADC. 256 snap frames are captured and integrated in a computer to maximize S/N. Global uniformity, local uniformity, bright pixel, black pixel, gorge and bundles of fiber interface are investigated. Pixel by pixel variation affects more than global variation on the centroiding accuracy.

[18] Dark current (hot pixel)
The input of the CCD camera is covered with a blackout material, and the light source in OGSE and the room lamp are turned off. The room te erature is set to 28 centigrade and the temperature of the ceramic package of the CCD is monitored by a stick-on thermocouple. The gain of the readout amplifier is increased by x10 of the normal setting, as the dark current signal may be small. 256 snap frames are captured and integrated in a computer to maximize S/N. Average dark current and global uniformity are investigate. Number distribution of dark current height is derived from all pixels. The number of hot pixels is counted. It must be confirmed there is no hot pixel in the black reference columns. As the output of hot pixel may fluctuate, this measurement is repeated 4 times in a 15min interval. A hot pixel affects most the centroiding accuracy.
Low transfer efficiency from V-CCD to H-CCD creates a vertical stripe in some devices. This pattern can be noticed from this high S/N dark frame, if it exists.
Periodic up and down pattern along horizontal direction is seen in some electronics system. Again, this pattern can be noticed from this high S/N dark frame, if it exists.

[19] Linearity of input v.s. output
e CCD camera is attached to the OGSE in the 3rd configuration with the relay lens x0.586 F/2. The green fluorescence panel is used as a light source. A rectangular graduated ND filter is put on the light box and wedge pattern is focused on the CCD. The illumination change along the position does not have to be exactly linear. 2 frames are observed with different brightness of the fluorescence panel, about 1.0 and 3.0. The ratio of the intensity is not necessary to be exact. One frame is divided by the other. If the relation of input vs. output of the CCD camera is described by the gamma curve, the ratio of the 2 frames is constant all over the CCD pixel(figures 19a and 19b). This simple measurement gives the deviation from the gamma curve for all points on the brightness axis. The deviation should be very small.
After the confirmation, the value of gamma is determined. ND filters 0.1, 0.2, 0.3, 0.4 and 0.65 have been calibrated accurately for the green fluorescence panel by the photon counting detector. Snap frames are taken putting the ND filters on the half area of the light box. The gamma value can be determined from ratios of the CCD outputs. As the stability of the light is 8% in the worst case, the half area of the CCD must see the light source directly to monitor the stability (figure 20).

[20] Readout noise and Conversion factor
Although the conversion factor of the on-chip amplifier is described by the CCD date sheet, the total conversion factor between electrons and ADC unit is not certain because the conversion factor itself changes with

temperature and band widths of the on-chip amplifier and readout electronics are not much faster than 10MHz. Therefore, the conversion factor in the total system must be determined by an experiment.

e total noise, n, is described by the combination of readout noise, rn, and the number of photo-electrons, p, as follows,

$$n^{2} = rn^{2} + p. \qquad (1)$$

where, n : total noise in units of electron
rn: readout noise in units of electron
p : number of photo-electron

If we re-write the above equation in units of ADC,

$$(c^{2})(N^{2})=(c^{2})(RN^{2}) + cP,$$

hence, $$N^{2} = RN^{2} + P/c, \qquad (2)$$

where, N : total noise in units of ADC
RN: readout noise in units of ADC
P : photo-electrons in units of ADC
c : conversion factor = ? electrons/ADC .

The equation(2) gives us straight line in the graph with the abscissa of output, P, and the ordinate of square of noise, N**2, which is named "photon transfer curve" (figure 21). The conversion factor can be derived from the gradient of the line. Once the conversion factor is determined, the readout noise is easily read from the ordinate at the abscissa P=0. The square root gives the readout noise. As the dynamic range of the ADC is only 8bit, it may be difficult to measure noise in the lower light level. The amplifier gain should be increased by x10 for the measurement of the lower part. The total noise, N, is measured from 2 contiguous frames with the same light level. As the time difference is short, the fluorecense panel illuminates in the same intensity, which of course can be checked by the observed frames. The subtraction of the 2 frames gives SQRT(2)*P. If the image of the rectangular graduated ND filter is projected on the CCD, different brightness, hence different noise, belt is seen in the CCD frame. Therefore, 2 frames are enough to make half of the photon transfer curve (the other half needs the change of the gain).

[2 Transfer Efficiency

The CCD camera is attached to the OGSE in the configuration shown in figure 1. The green fluorescence panel and 11x11 pinhole array with 27um diameter are used to project a 5.5um pinhole on the CCD. The transfer efficiency is better in the brighter light level and in positions closer to the output. The light level is turned up so as that the peak brightness of the pinhole is 80% of the full scale of the ADC. The pinhole images are delivered close to the output part of the CCD, and 128 snap frames are captured and integrated in a computer. The wing feature may appear around 3x3 CCD pixel, which is caused by the scattering at the fiber interface and CCD surface and is the reference for the real measurement.
The light level is turned down to 30% of full scale of the ADC, which simulate real event energy, and the pinhole image is delivered to the far end of the CCD. 256 snap frames are captured and integrated in a computer. The wing features at neighbouring CCD pixels particularly far side are investigated carefully. The light level is turned down to 10 ADC unit and then the gain of the readout amplifier is increased by x10 for compensation. Another 256 snap frames are captured and integrated in a computer and neighbouring pixels are investigated. The last experiment is a more severe situation than the real.

[22] Amplifier speed

The output signal of CCD is monitored by a 400MHz oscilloscope with the slower clock of 1MHz. The settling time of the on-chip amplifier is measured from the decay speed of the signal profile corresponding to a single pixel.

[2] Systematic electric noise

Digitization interval is not always constant, for instance even numbers dominate odd numbers in some electronics system. The image of the rectangular graduated ND filter is analysed and the number distribution is derived. It should be confirmed that no systematic distribution is seen.

[24] Sensitivity uniformity within a pixel

This is an optional item, but is worth trying. The CCD camera is attached to the OGSE in the configuration shown in figure 1. A 12um pinhole is stuck on the mask and projected on the CCD. If the green fluorescence panel is used, the image size is 2.5um. The image is moved in a step of 0.5umx0.5um over the full pixel area. The fine structure of sensitivity is derived.

IV. Total Performance at high count rate

[25] Linearity

e response of the blue detector to a diffuse source is measured with the monochrometer, as the monochrometer can create a 1mm round image on the detector and also contains the photomultiplier. The measurement sequence is same as [8], but with a halogen lamp and with a fixed wavelength of 500nm. The brightness of the halogen lamp is gradually increased from 0 to 1million count/sec over the full detector area. The outputs of the blue detector are compared with that of the photomultiplier. The linearity is expected to be limited by the frame rate of the readout system. But, unknown phenomena will happen in VUV region, where multiple photo-electrons are generated at the photocathode. Therefore, the same test is performed at 170nm using the deuterium lamp. The light level is controlled by slit width and the attenuater.

The response to the point source is not limited only by the readout speed but also the image intensifier (pore paralysis). The gain depletion for the high count rate of a point source is already measured in [1], but overall performance is tested again here. The blue detector is attached to the OGSE with the configuration shown in figure 1. A 5(H)x8(V) pinhole array will be newly made. It consists 27um pinhole with different brightness and a large dense window (e.g. ND3.0) for mo toring the light source. The mask pattern is projected on the detector with the green fluorescence panel. The brightness of pinhole is calibrated with very low count rate first of all. Then, the ratios of brightnesses among pinhole are measured with different light levels. The light level is accurately monitored through the window, as the count rate is very low in the dense window but there are enough photons because of the large area.

[26] Coincidence

The effect of overlapping events with high count rate is one of the most crucial problems in the blue detector. The strong grid pattern in a sky background associated with CCD pixel and square dark region around a bright star are expected by simulation (figure 22), and are also actually observed. A new algorithm, parabola fitting, and the round and smaller event size will hopefully overcome the problem, but must be tested in several situations.

A) Sky vs. sky

A flat field image is observed in 2048x2048 pixel format for the light level of 200 000 counts/sec over the detector area. It should be confirmed that the grid pattern is less than 10% and can be corrected by software without the loss of position accuracy.

B) Star on sky

Bright stars (pinholes) with a size of 5.5um are projected on the detector using the configuration shown in figure 1. The distance of the black zone is investigated against the sky background of 200 000 count/sec. The pattern variation is also investigated with the position of the star within a CCD pixel, which can be achieved by using the x-y table.

C) tar on sky

The size of a medium brightness star is investigated in the same setting as above with and without the background. Again, the change of the size and the center of gravity with the position of the star within a CCD pixel is investigated.

D) Star v.s. star

A 5x5 double star array, which contains pair pinholes with different separations and different azimuth angles, are projected on the detector. The features are investigated in the low and the high light level. The change of feature is also investigated for the different places of the pair star position within a CCD pixel.

[27] Time resolution

A colour slide image, which contains blue and red stars with various brightnesses, is projected on the detector using the blue and red LEDs. The intensities of the LEDs are changed as follows,

R=DCr + R1*sin(Fr1*t) + R2*sin(Fr2*t)
and
B=DCb + B1*sin(Fb1*t) + B2*sin(Fb2*t) .

Typical example is
R1/DCr=1-10%, R2/DCr=100-300%, Fr1=1-10ms, Fr2=1-10hours
and
B=const.

Blue stars can be used as standard stars in the example. The twinkling stellar image is observed and analysed by the DPU in the fast mode. The fast mode is confirmed by comparing the derived Fourier component and the electrically created one.

[28] Field test of blue detector

We sometimes make a crucial mistake or misunderstanding, which are difficult to notice in the laboratory. Field application, particularly photometry of standard stars, with our system would give further proof of our experiment. As the requirement of cleanliness is severe, the DEP straight tube, which was made for development, is brought to the field. A candidate for the telescope is the small telescope in the back yard of MS . Standard stars and variable starts are observed with the "Blue Detector+IBM-PC". Examples of object and aim are,

1) standard star for sensitivity and S/N
2) open cluster, e.g. Pleiades, Praesepe for astrometric and photometric accuracies.
3) variable stars for the time resolution and stability
e.g.
Crab Pulsar (P=30ms)
Central star of planetary nebula (P=1 hour)
AM Her stars (P=0.1 day)

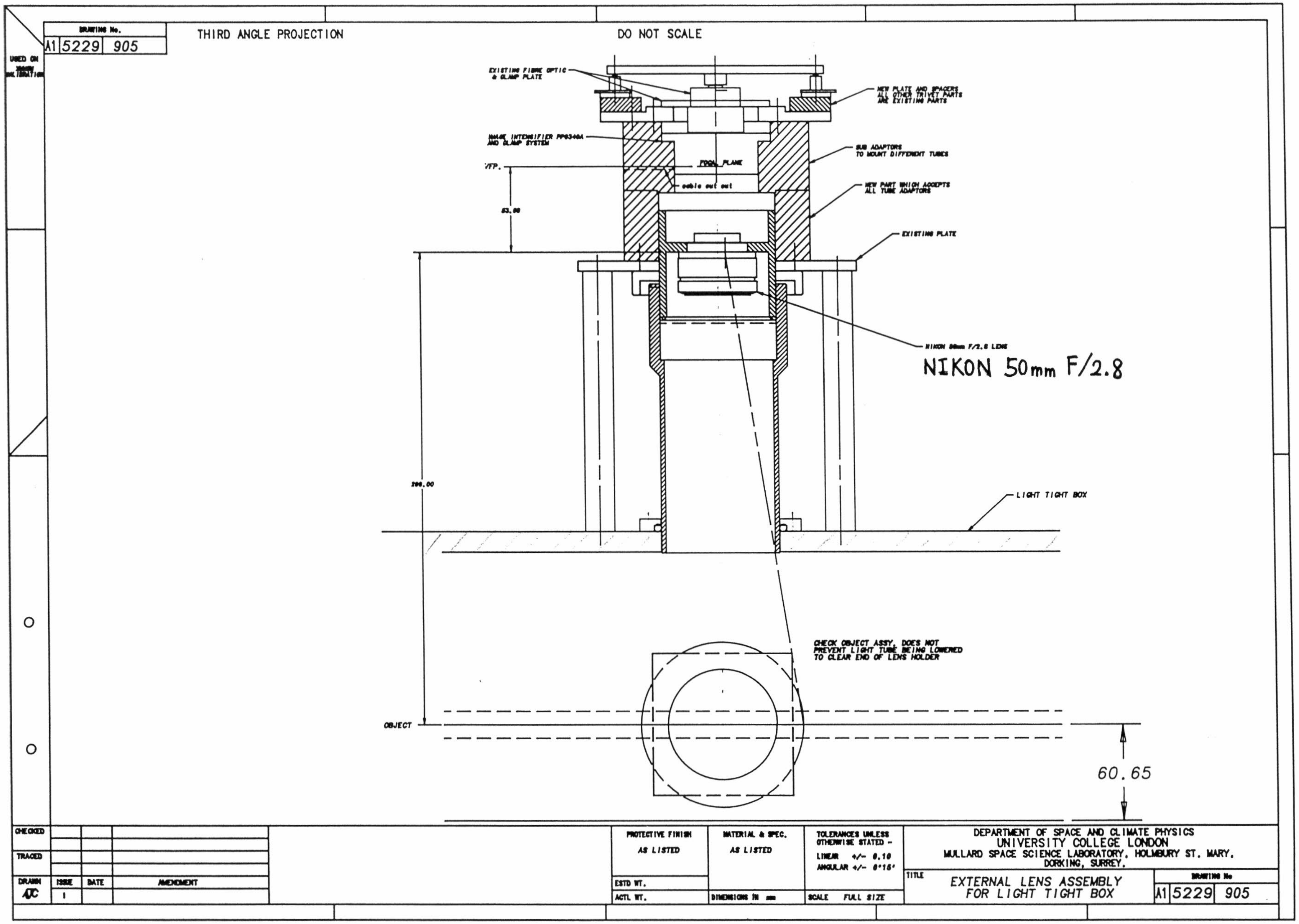

Figure 1. OGSE for resolution test. Spot size of pinhole array is 5.5um on the detector. The local position accuracy on the detector is 0.16um

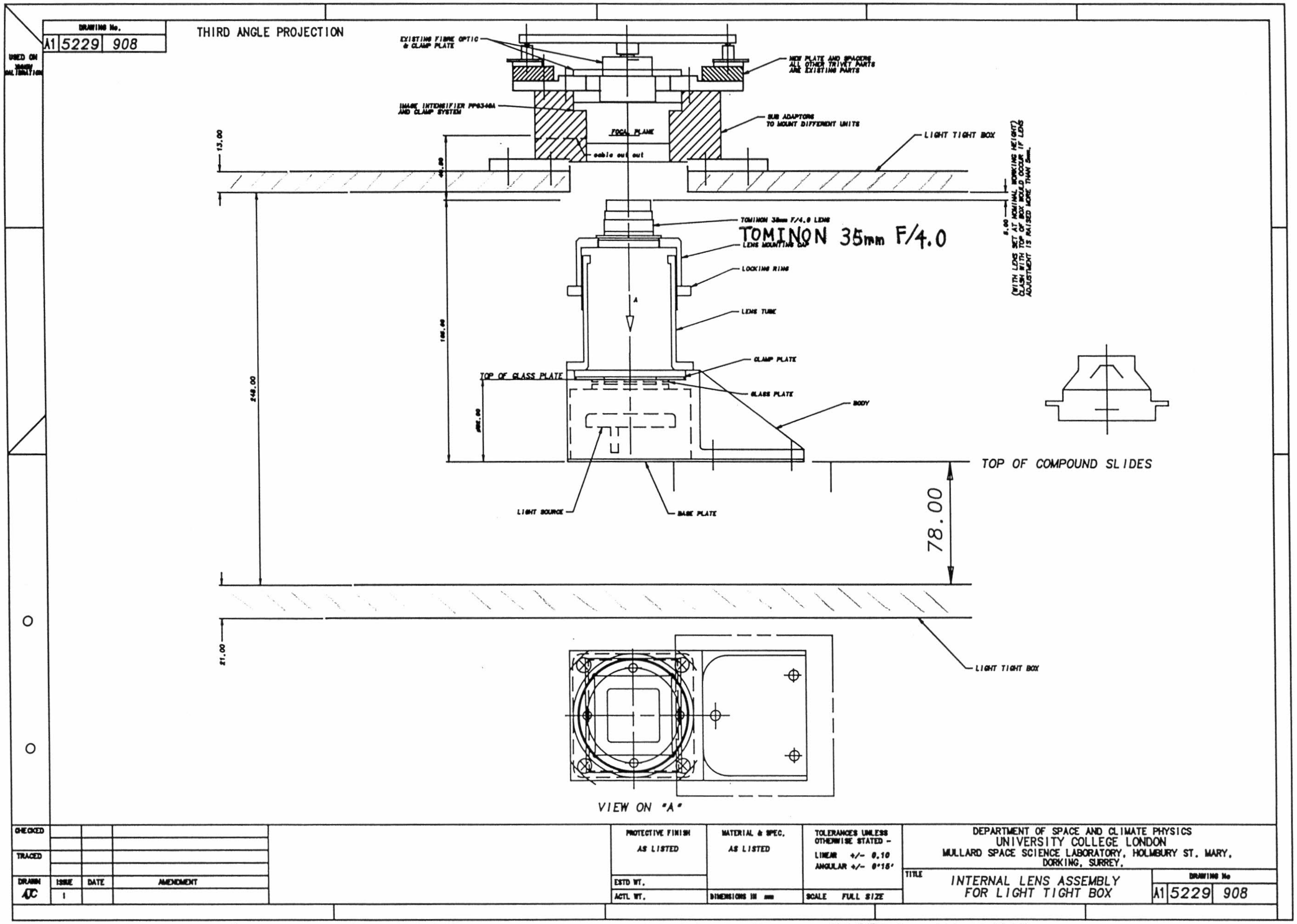

Figure 2. OGSE for global distortion test. The position accuracy is 1um over 25mm.

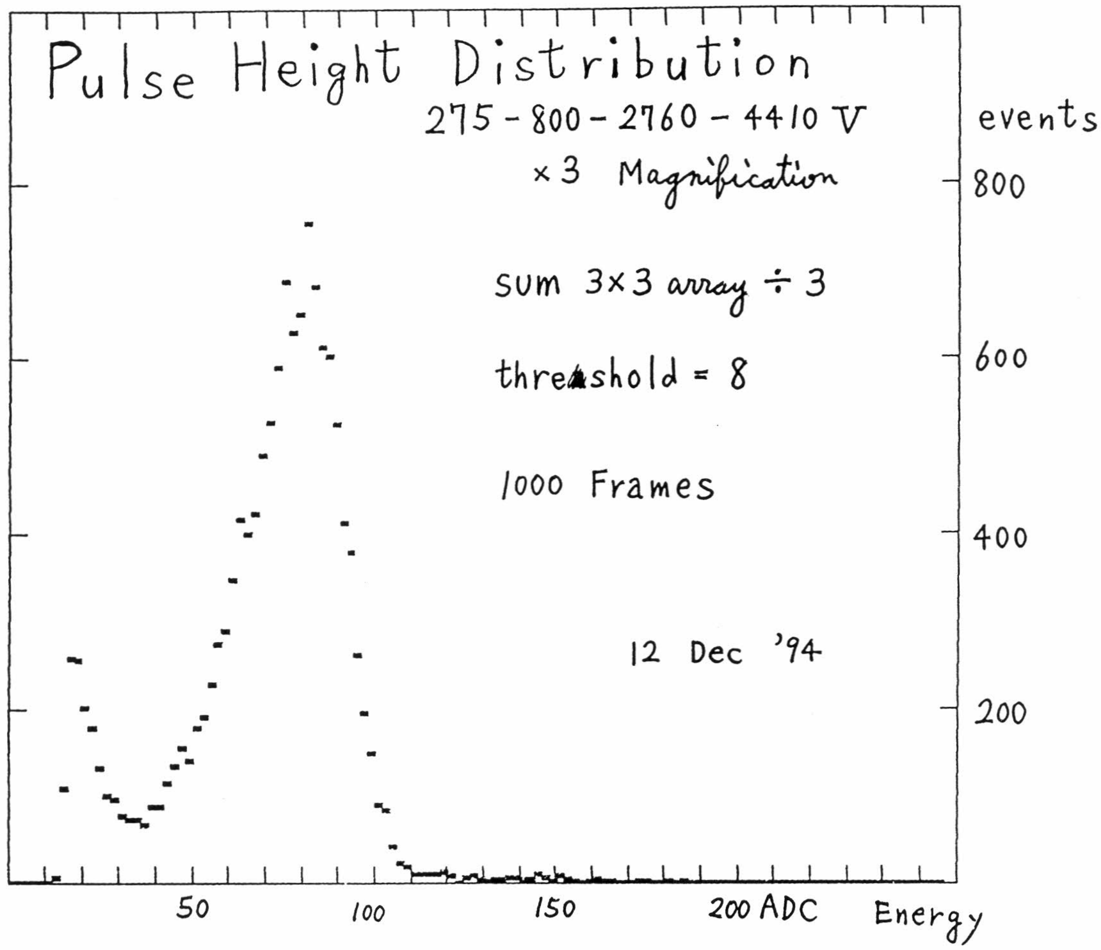

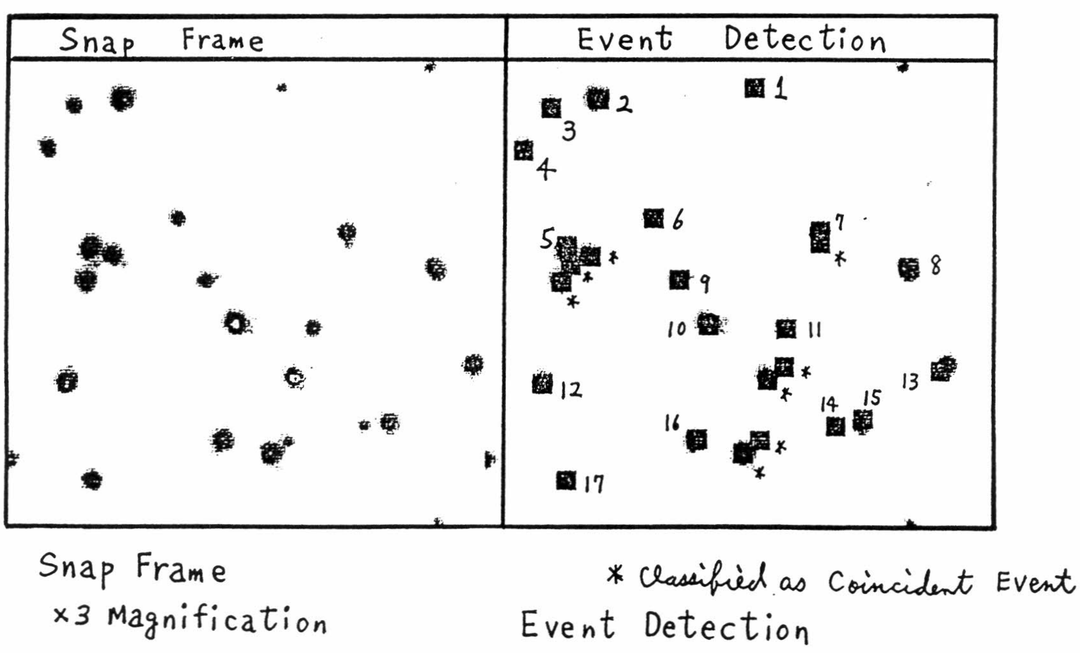

Figure 3. Pulse height distribution of DEP-staright tube. The lower panel shows an original CCD snap frame and its event detection by a computer.

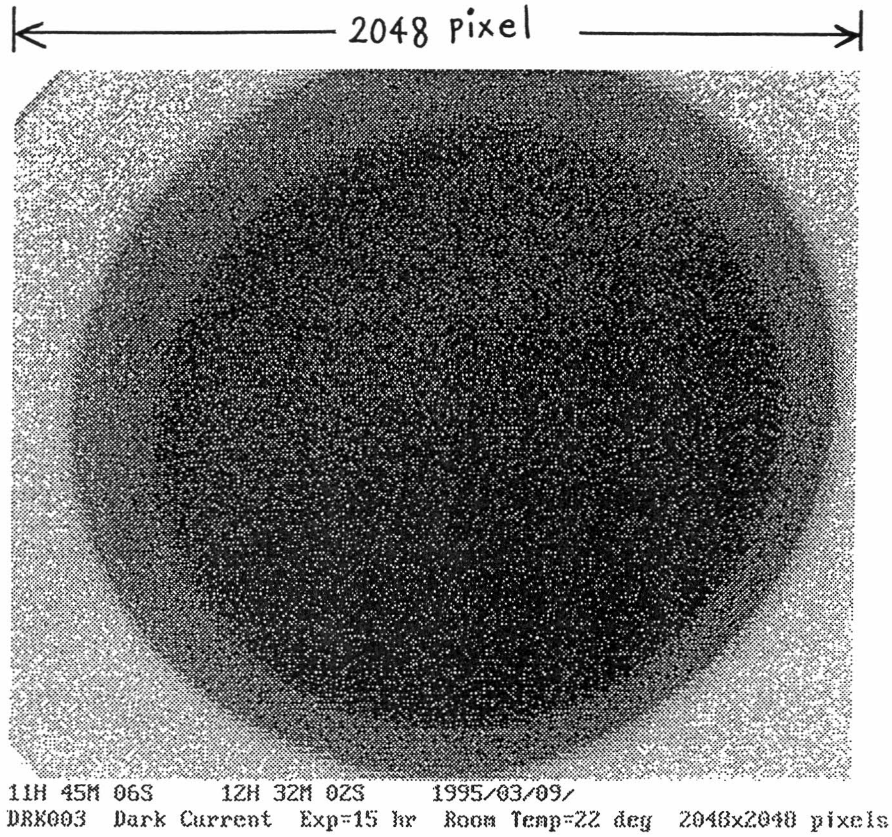

Figure 4. Dark current of DEP-taper incorporated tube with an exposure time of 15 hours. Top and bottom of left hand side corner show the edge of the tube.

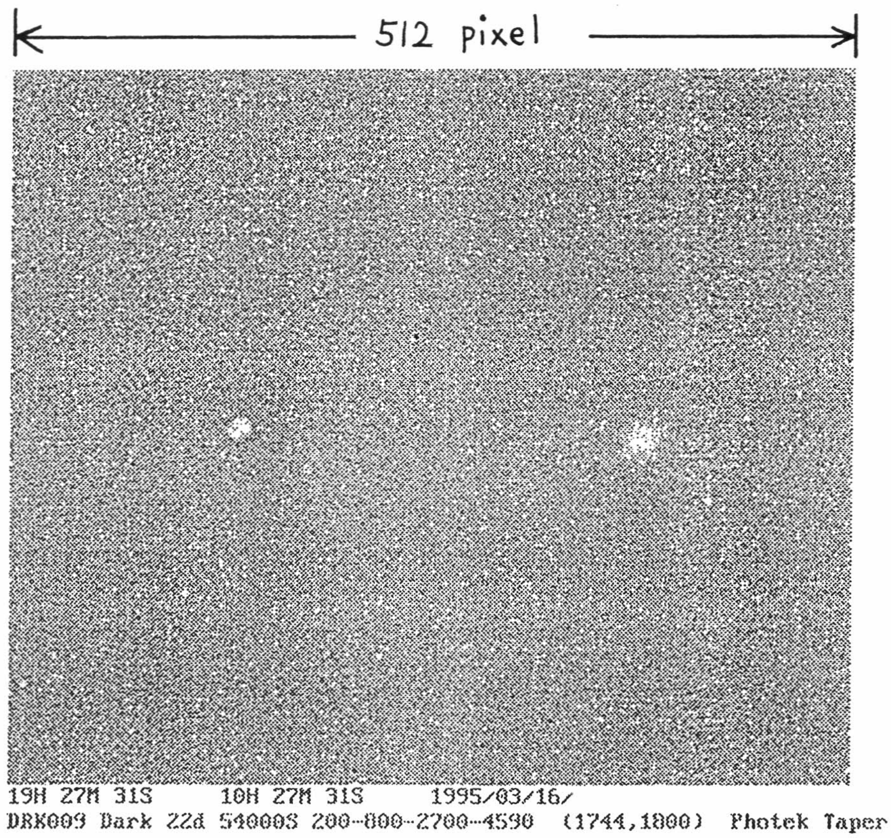

Figure 5. Dead pores of Photek-taper incorporated tube shown in the dark current image integrated for 15 hours.

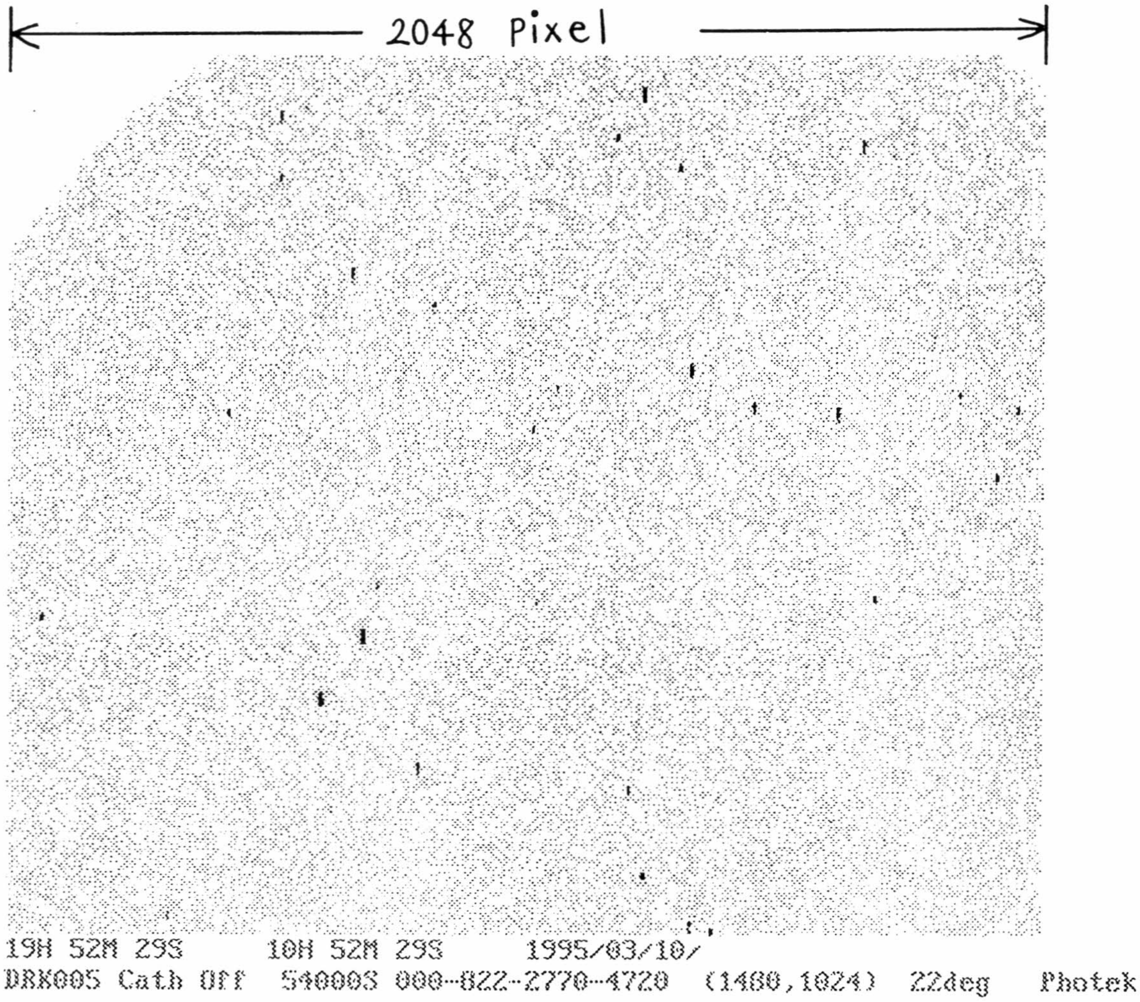

Figure 6. Turn-on Channel of Photek-taper incorporated tube shown in the 15 hours exposure frame with photo-cathode OFF.

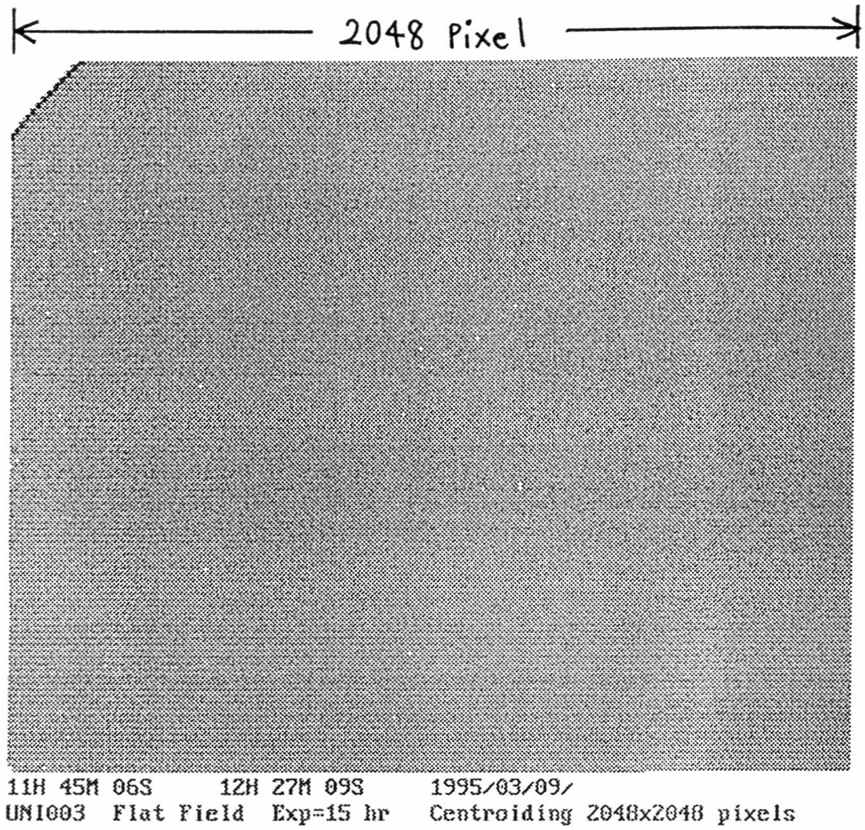

Figure 7. Flat field image (photon counting mode) of DEP-taper incorporated tube in the low count rate with the exposure time of 15 hours. One pixel corresponds to 9.7um on the phosphor screen.

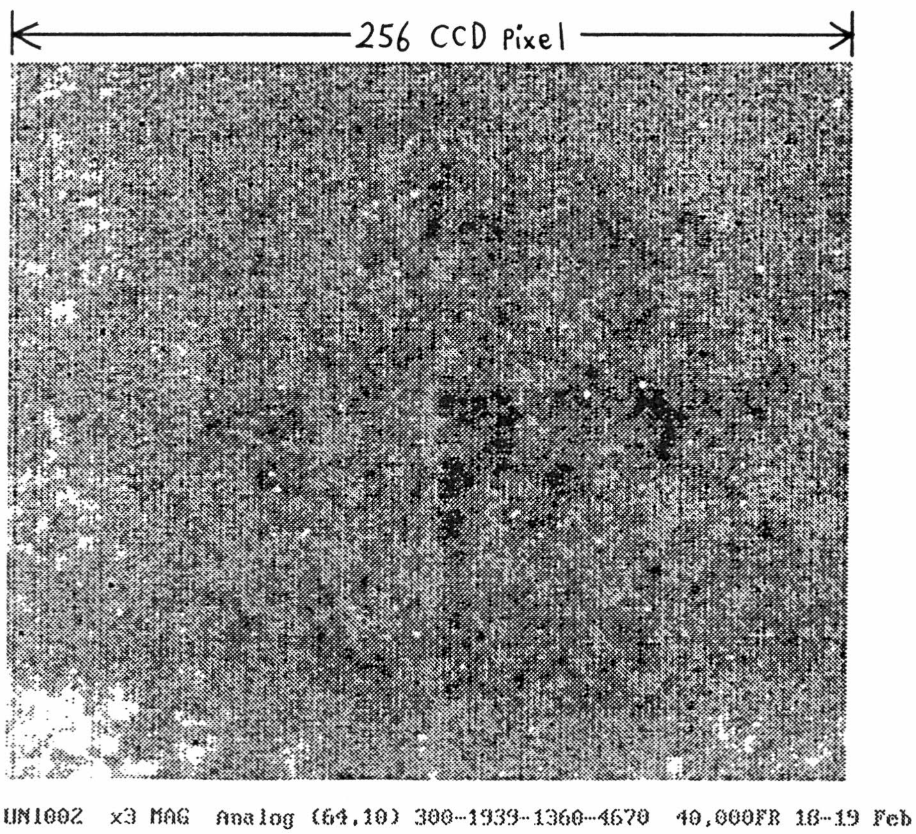

Figure 8. Flat field image (analog mode) of DEP-taper incorporated tube in the low count rate summing up 40,000 CCD snap frames. One CCD pixel corresponds 21um on the phosphor screen.

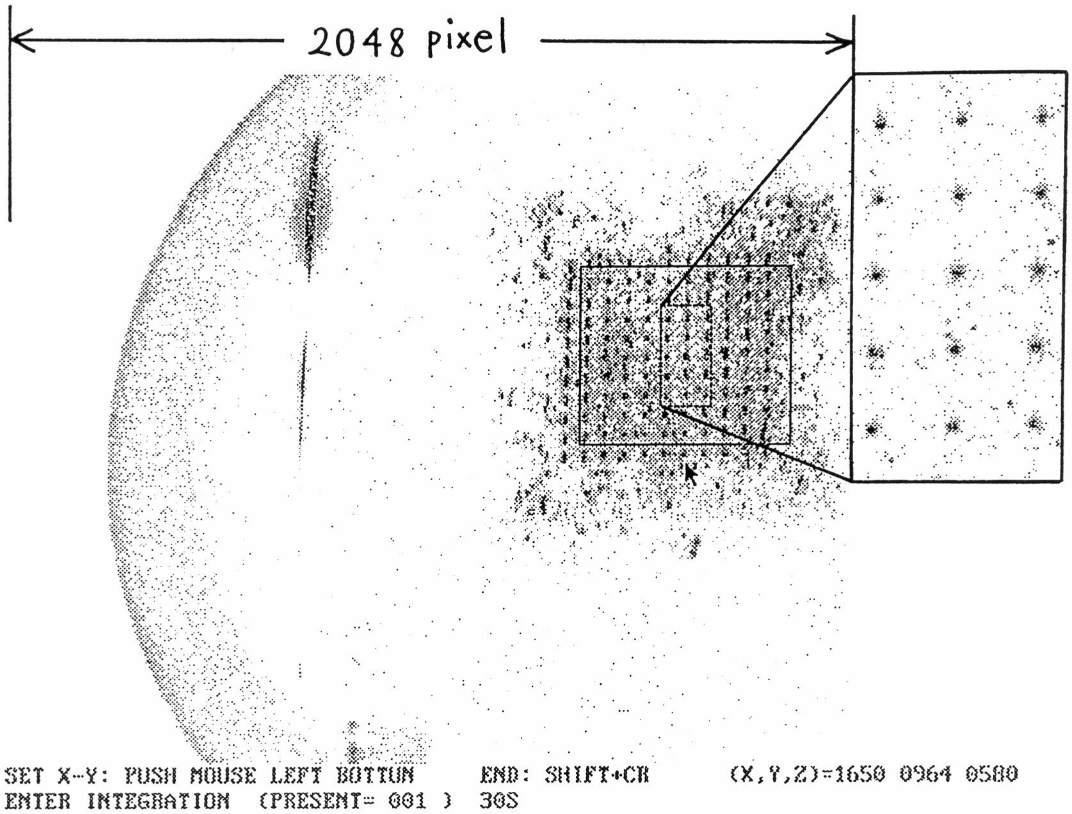

Figure 9. Pinhole array projected on the detector. The central 5x5 array is used for the resolution test. The circle in the left hand side shows the edge of the tube.

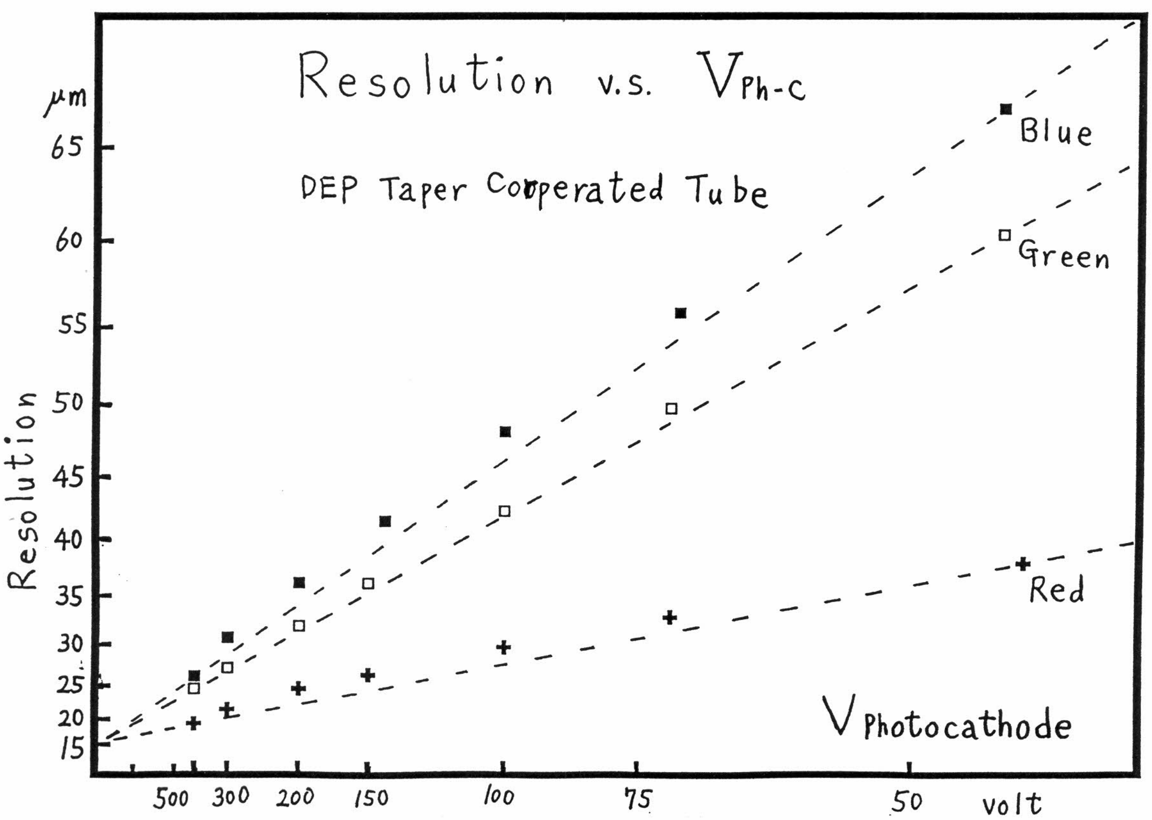

Figure 10. Resolution vs. photo-cathode voltage for different colours. The resolution is better for the light of the longer wavelength and for the higher photo-cathode voltage.

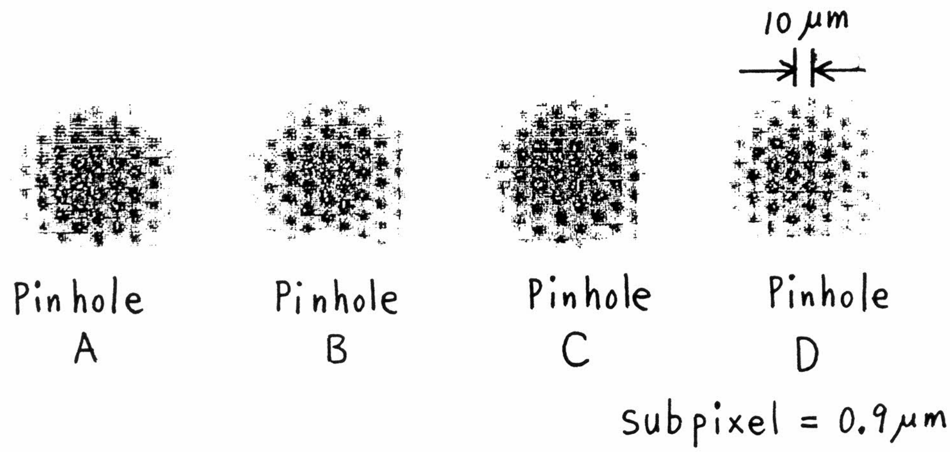

Figure 11. MCP pore structure of DEP-straight tube. 1 million CCD snap frames were analysed by software and are mapped into 0.9um subpixel. As only 80V was applied to the photo-cathode gap, pinhole images themselves were blurred.

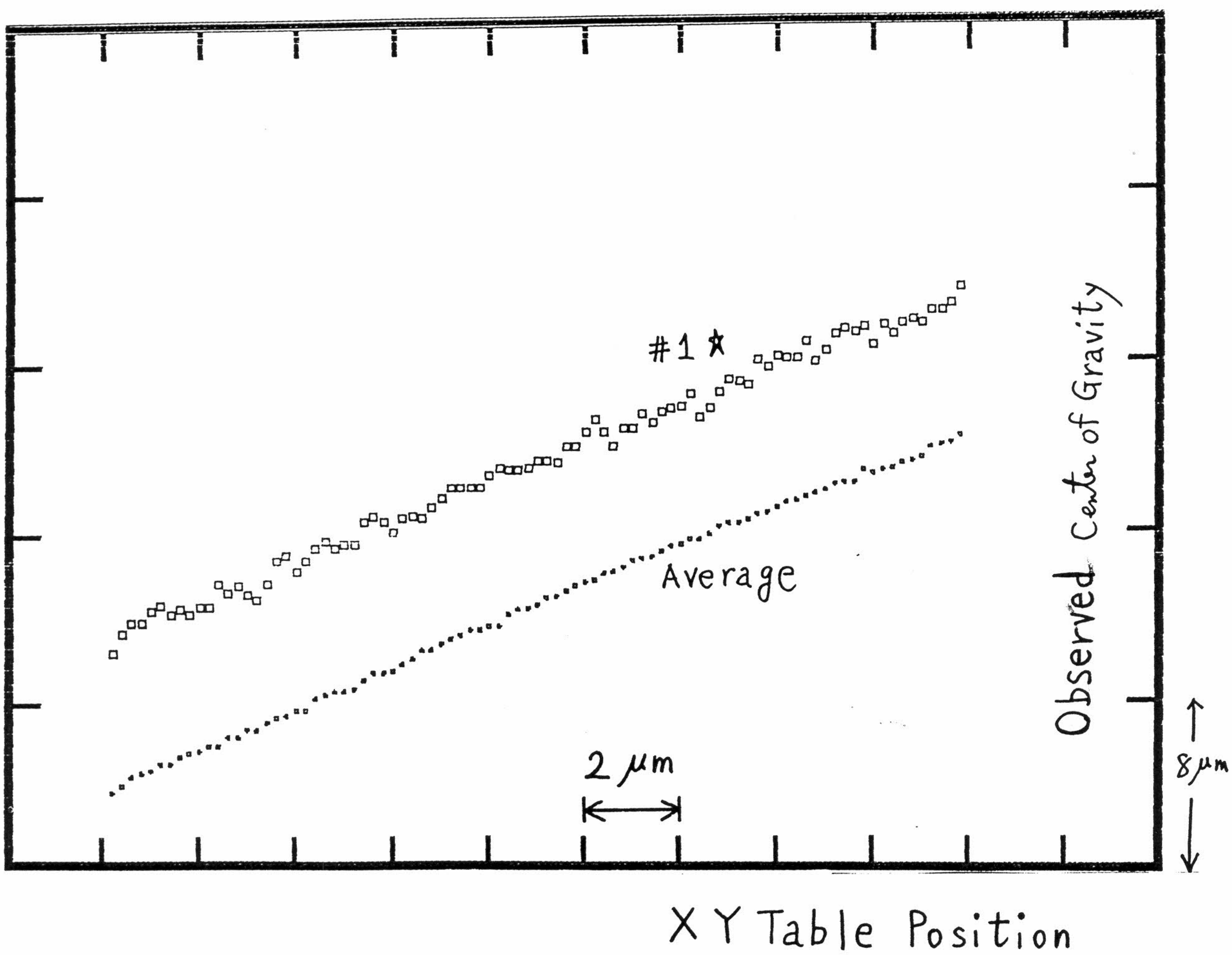

Figure 12. Position accuracy over 20um travel. Average was derived from positions of 16 starts.

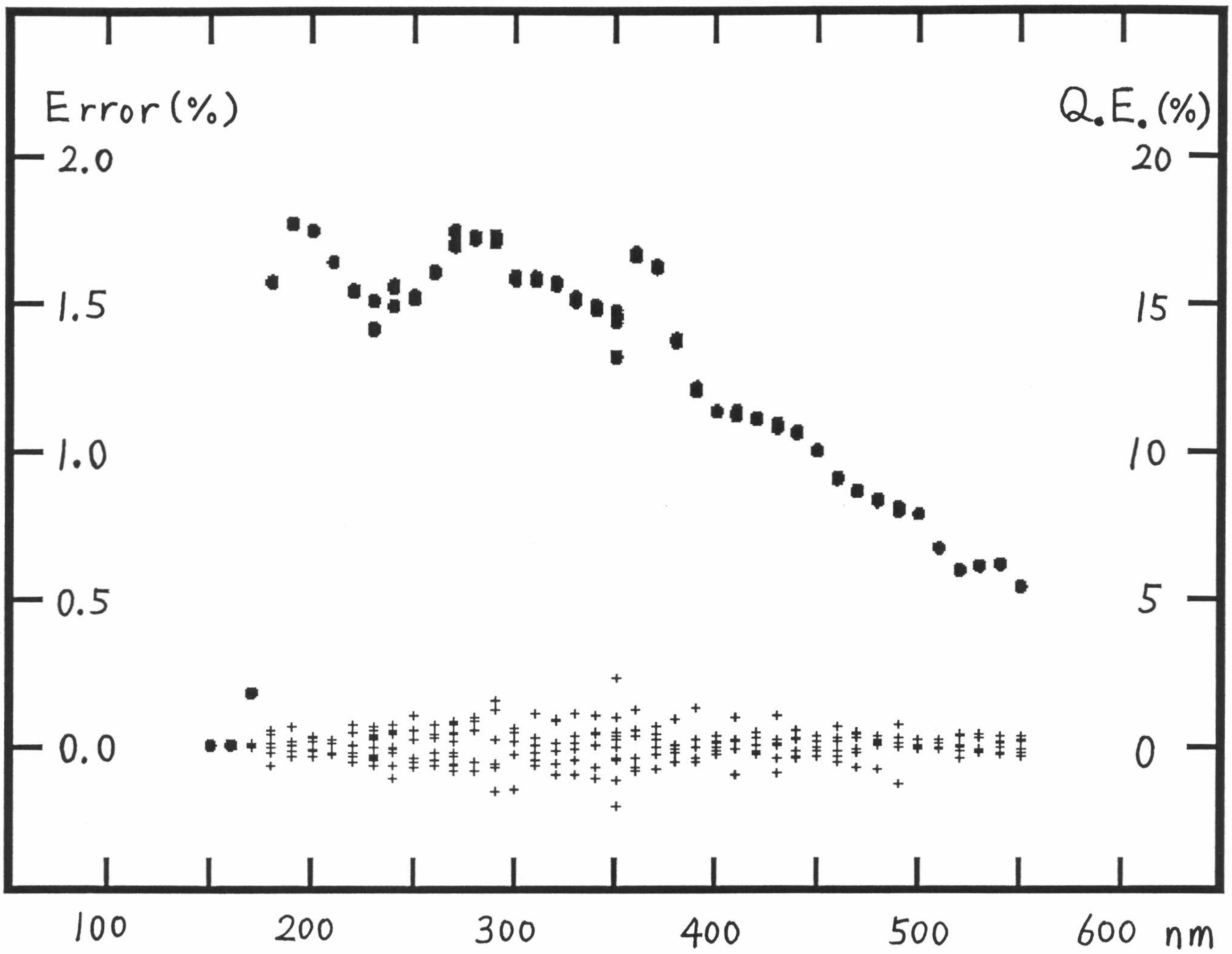

Figure 13. Detectable quantum efficiency of the blue detector. Filled circle shows the Q.E., and crosses show discrepancies among the 6 redundant measurements.

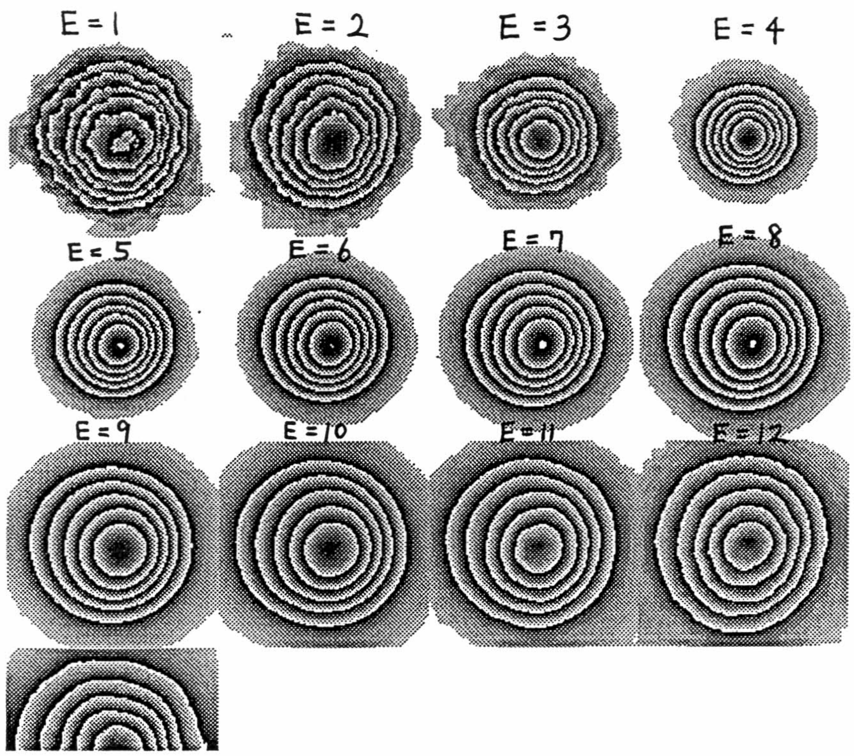

Figure 14. Standard event profiles of DEP-straight tube for different energies.

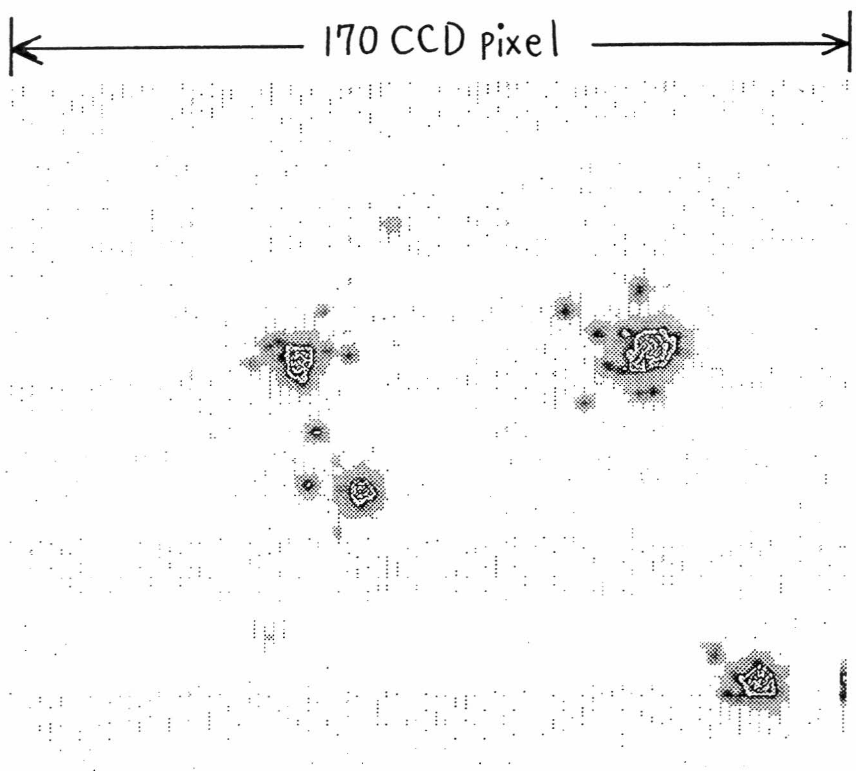

Figure 15. Satellite events of DEP development tube-A captured in a CCD snap frame. One CCD pixel corresponds 23um on the phosphor screen.

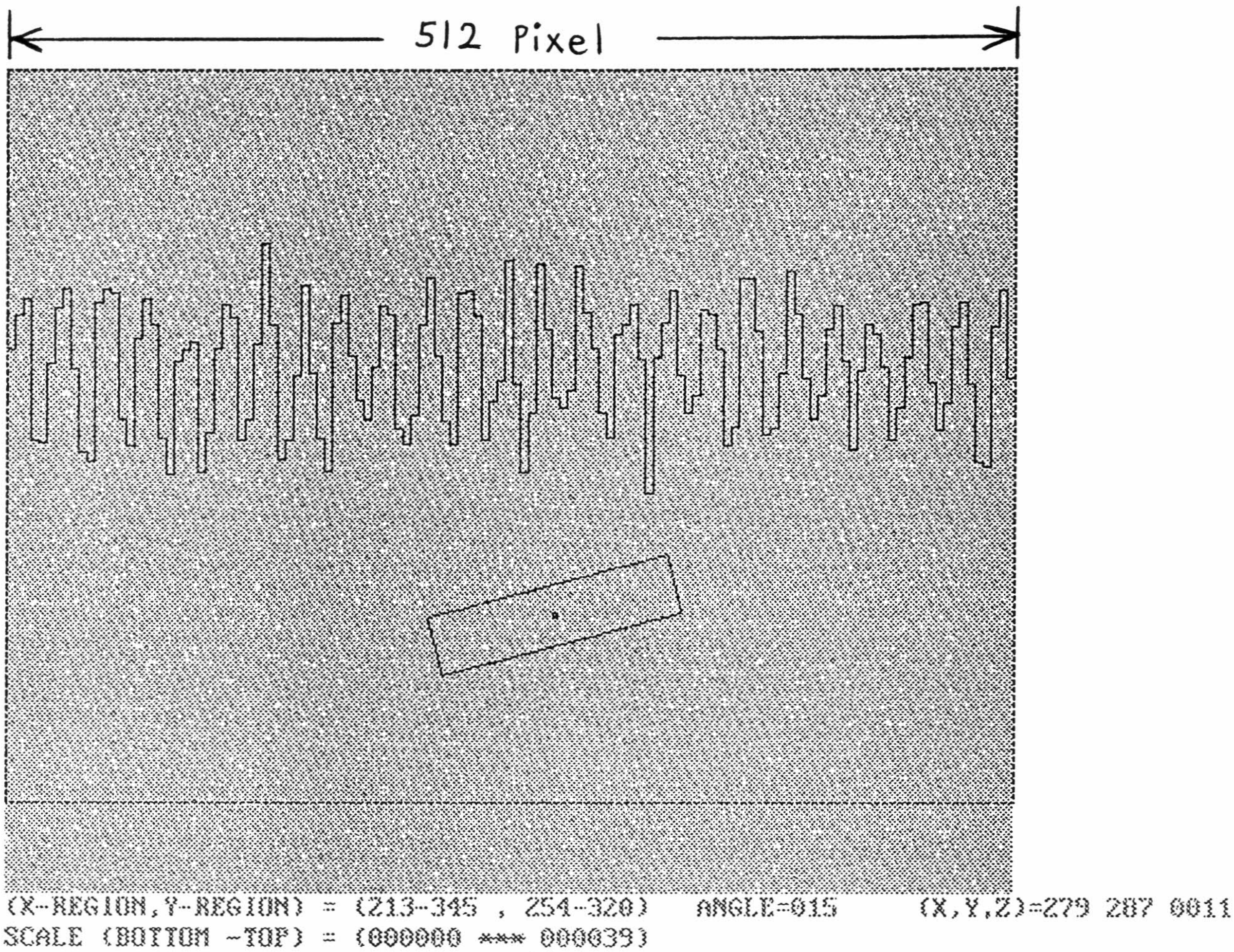

Figure 16. Moire fringing of DEP-taper incorporated tube. Systematic pattern runs along azimuth=105 degree.

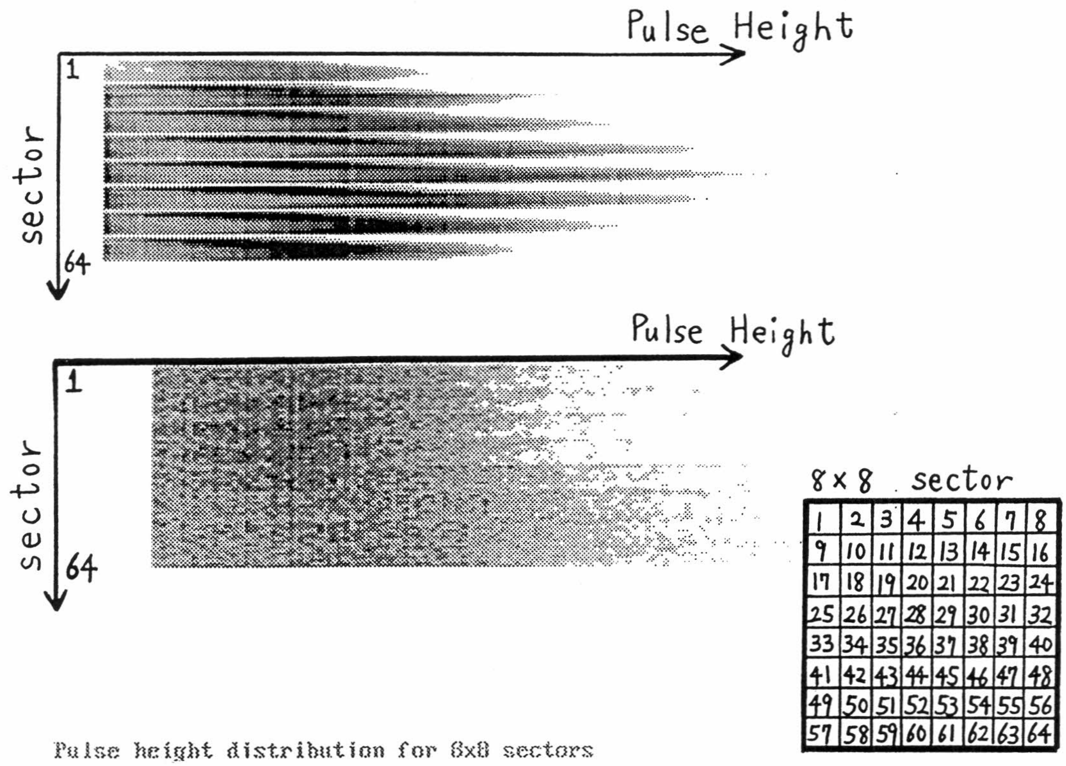

Figure 17. Gray scale display of pulse height distributions for different places (8x8 sectors). The upper panel, DEP-taper incorporated tube, shows strong non-uniformity. While the lower panel, Photek-taper incorporated tube, fairly uniform.

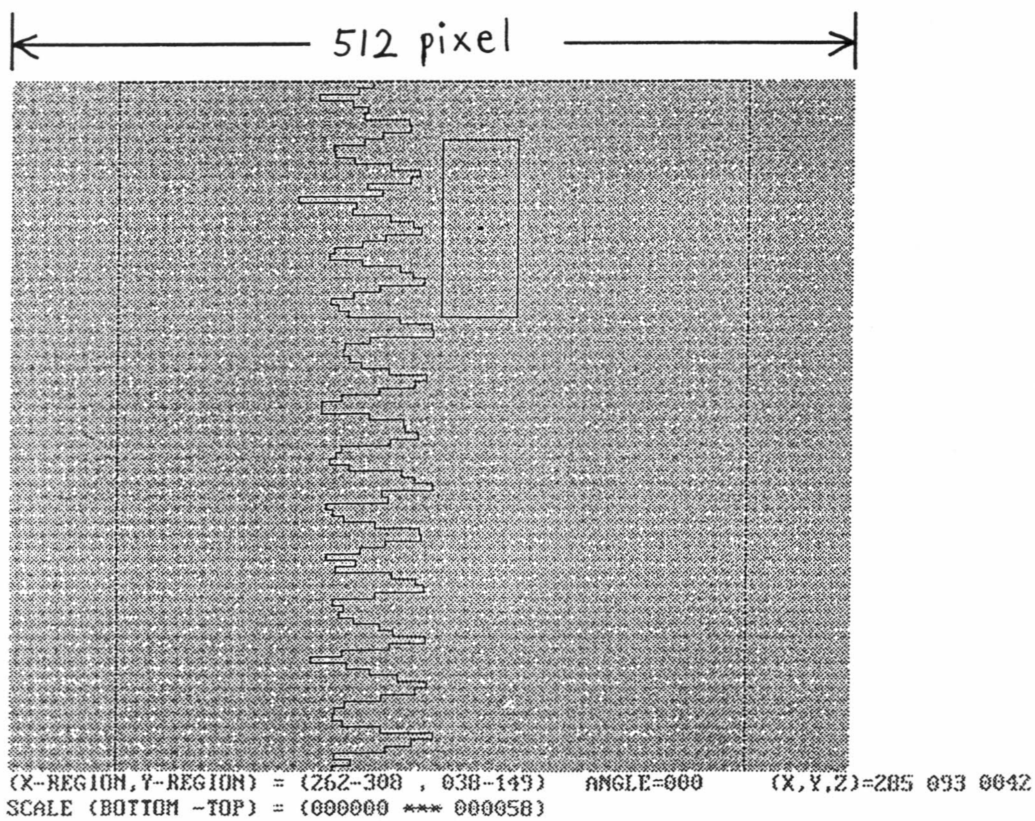

Figure 18. Flat field image of DEP-taper incorporated tube at the edge of the detector, when the centroiding LUT was tuned at the center. CCD pixel based modulation pattern appears due to the spatial variation of event profile.

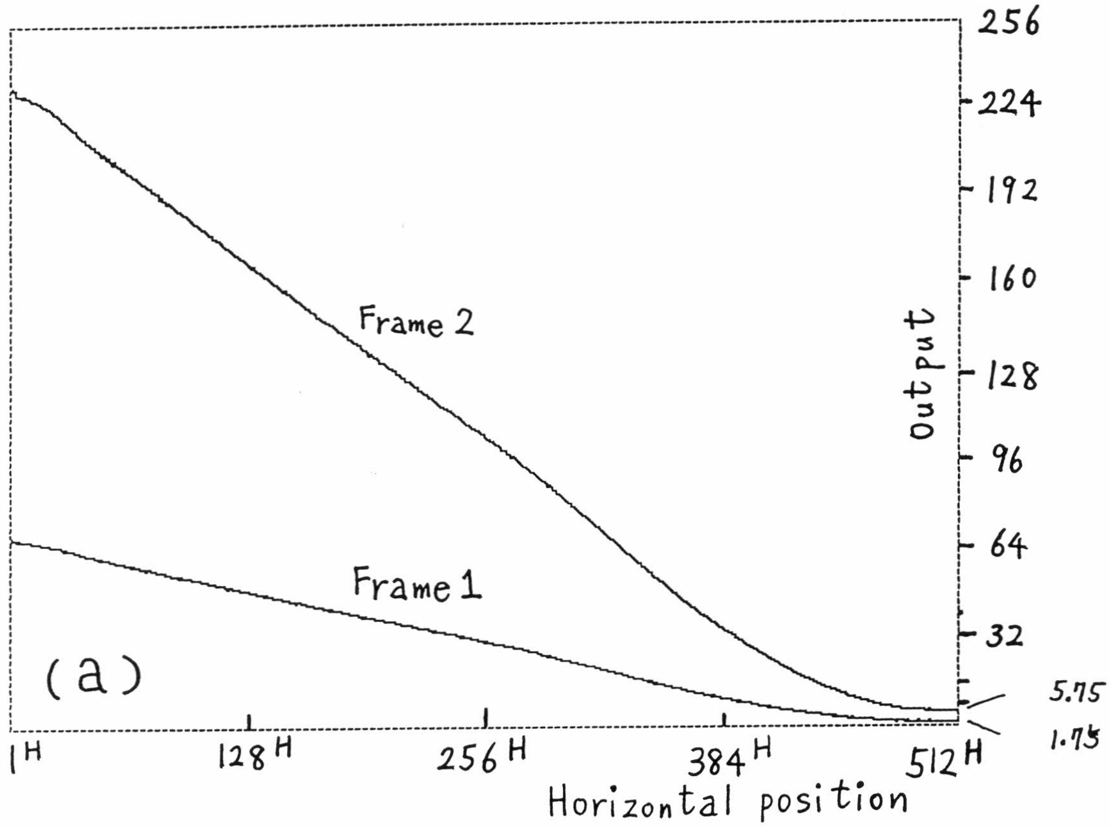

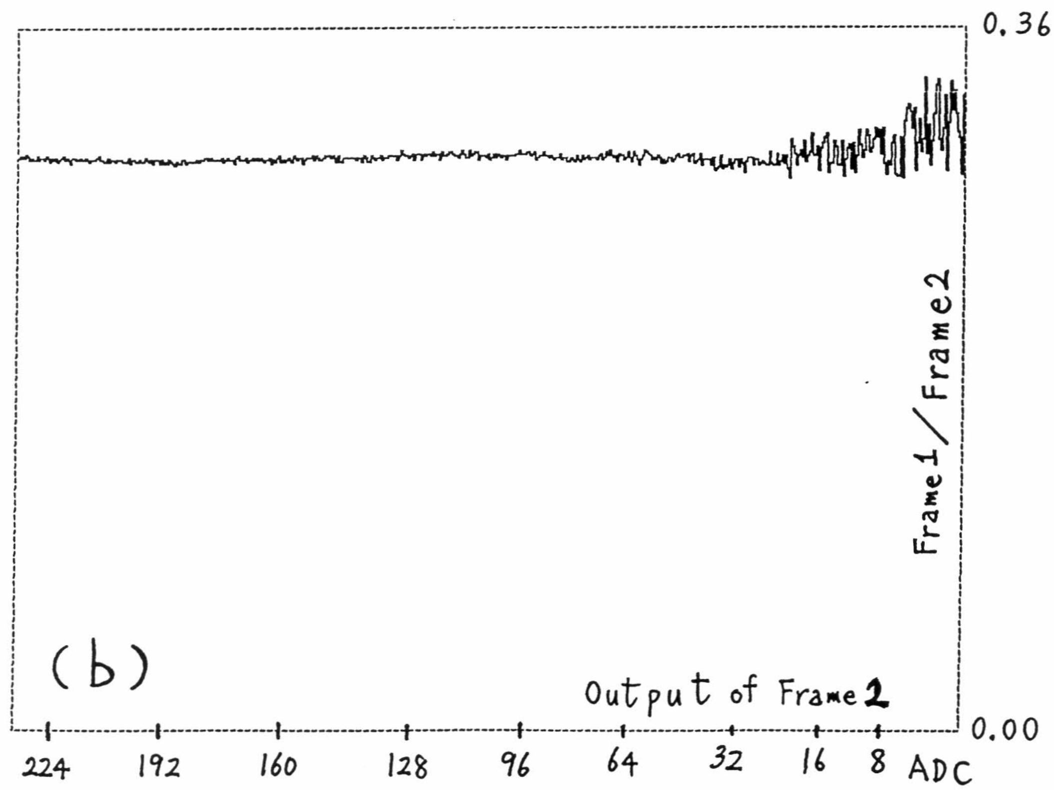

Figure 19 Linearity test of SONY CCD camera. (a) The change of brightness along the horizontal direction in 2 frames. (b) The ratio of the 2 frames at different light levels.

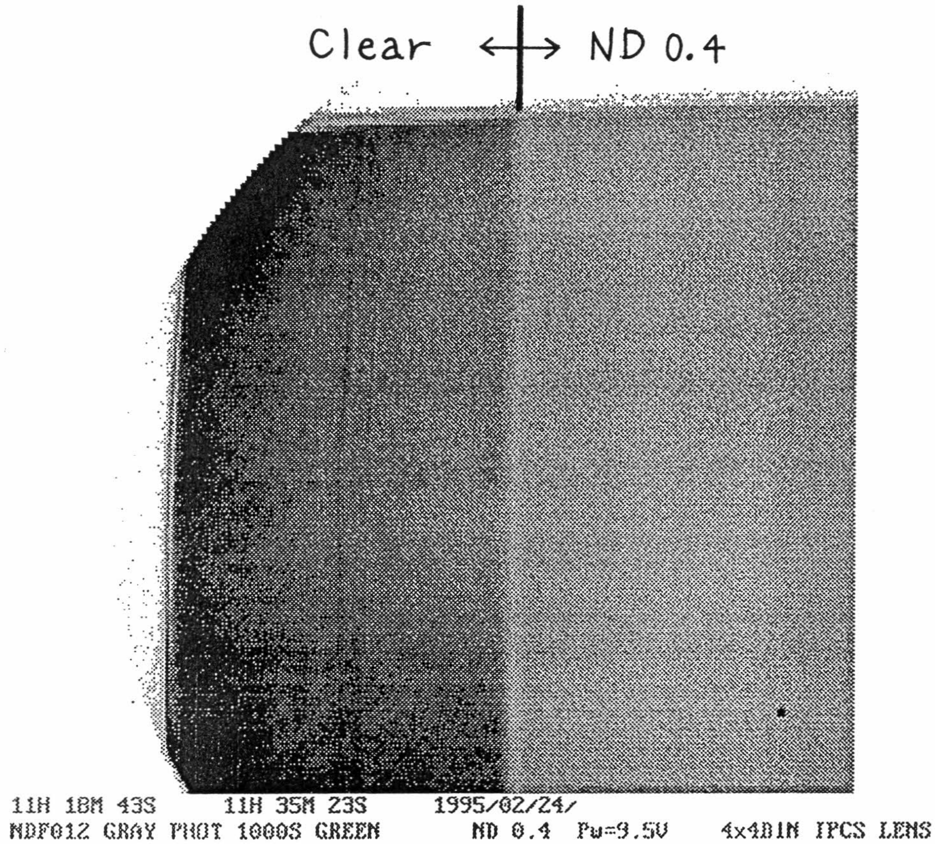

Figure 20. Calibration of a ND filter by the blue detector.

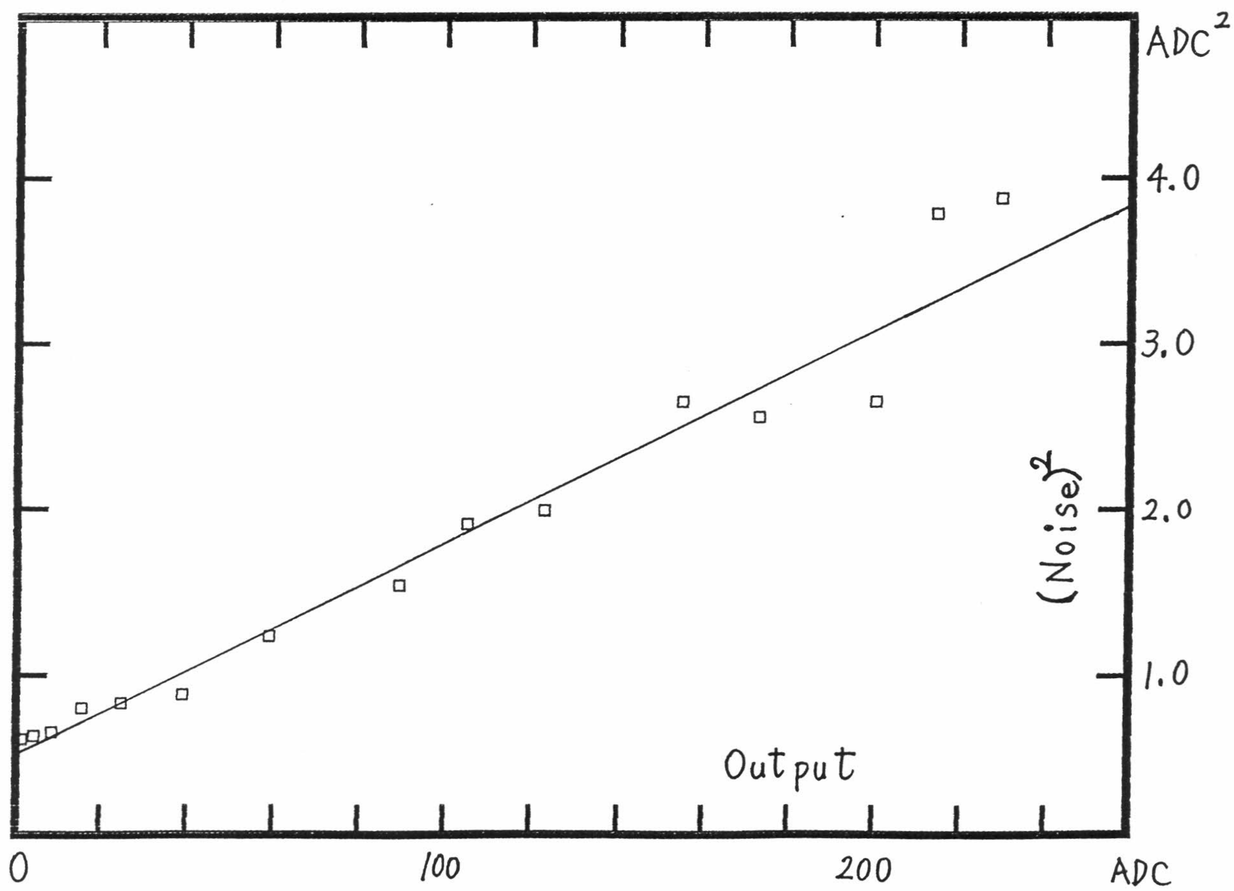

Figure 21. Photon transfer curve for SONY CCD camera. The gradient of the curve gives the conversion factor, and the offset from the origin the readout noise.

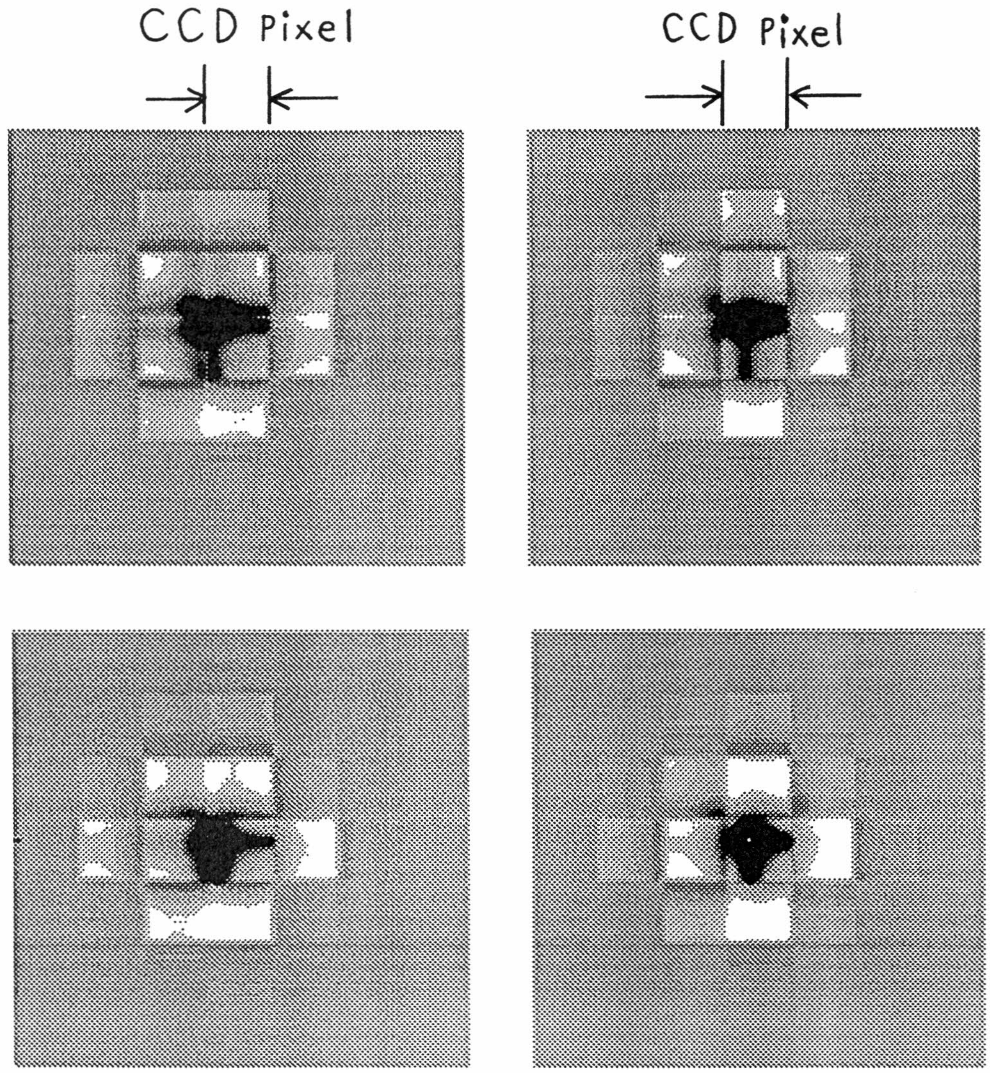

Figure 22. Simulation of coincidence between a star and sky background. The stellar positions within the CCD pixel are (0.125,0.125), (0.375,0.125), (0.375,0.375) and (0.125,0.375) clockwise from the top left.